Letter **Editors' Suggestion** **Featured in Physics**

Why mercury is a superconductor

Cesare Tresca[1,2,3] Gianni Profeta[1,3] Giovanni Marini,[1] Giovanni B. Bachelet[2] Antonio Sanna,[4] Matteo Calandra,[5,6] and Lilia Boeri[2]

[1]*Department of Physical and Chemical Sciences, University of L'Aquila, Via Vetoio 10, I-67100 L'Aquila, Italy*
[2]*Dipartimento di Fisica, Sapienza Università di Roma, 00185 Roma, Italy*
[3]*CNR-SPIN, University of L'Aquila, Via Vetoio 10, I-67100 L'Aquila, Italy*
[4]*Max-Planck-Institut für Mikrostrukturphysik, Weinberg 2, D-06120 Halle, Germany*
[5]*Sorbonne Université, CNRS, Institut des Nanosciences de Paris, UMR 7588, F-75252 Paris, France*
[6]*Department of Physics, University of Trento, Via Sommarive 14, 38123 Povo, Italy*

Despite being the oldest known superconductor, solid mercury is mysteriously absent from all current computational databases of superconductors. In this Research Letter, we present a critical study of its superconducting properties based on state-of-the-art superconducting density functional theory. Our calculations reveal numerous anomalies in electronic and lattice properties, which can mostly be handled, with due care, by modern *ab initio* techniques. In particular, we highlight an anomalous role of spin-orbit coupling in the dynamical stability and of semicore *d* levels in the effective Coulomb interaction and, ultimately, the critical temperature.

In 1911, Kamerlingh Onnes [1], investigating the transport properties of mercury at low temperatures, observed for the first time a superconducting (SC) transition: Below a critical temperature $T_c = 4.15$ K, the electrical resistivity dropped to zero. The discovery marked a milestone in physics history. The first microscopic theory of this phenomenon was formulated only 50 years later by Bardeen, Cooper, and Schrieffer (BCS) [2]. Their theory, refined through the Migdal-Éliashberg (ME) [3,4] Green's function formalism and the Morel and Anderson Coulomb pseudopotential μ^* [5], permitted an accurate picture of the normal phase and the SC phase of conventional (phonon-mediated) superconductors to be drawn.

In the 1960s and 1970s, when an *ab initio* solution of the Éliashberg equations was beyond available computational capabilities, mercury, among others, served as a benchmark to derive approximate analytical expressions for various superconducting properties, whose main ingredients were extracted from experiments. Normal-state electronic structure was inferred from de Haas–van Alphen [6], magnetoresistance, and cyclotron-resonance measurements [7,8]; phonon dispersion curves were inferred from neutron inelastic scattering [9]; and the Éliashberg function $\alpha^2 F(\omega)$ and the SC gap were inferred from tunneling experiments [10,11]. Notable examples are the McMillan-Allen-Dynes [12,13] approximate formulas for T_c.

Towards the end of the century, progress in density functional (perturbation) theory [14] allowed first-principles calculations of the electron-phonon spectral function [15] and superconducting T_c's and gaps [16,17]. These methods, combined with modern crystal-structure prediction algorithms [18–22] and with Ashcroft's intuition of high-T_c SC in hydrogen-rich metallic alloys [23], were the driving force behind the *hydride rush* of the last five years [22,24].

Following these achievements, methods based on density functional theory (DFT) are rapidly becoming the tool of choice to guide new superconductor discoveries. The field is evolving in the direction of high-throughput material design; this requires extensive benchmarks on known materials to vouch the accuracy of current theoretical or computational methods. The first results seem encouraging: For most conventional superconductors, the agreement between different theoretical approaches and experiment is remarkable [15,17,25]. However, a few notable exceptions exist. In particular, a close inspection of the available literature reveals that mercury is inexplicably absent from all currently accessible benchmark calculations.

This Research Letter reports our attempt to fill this gap. In particular, we address the following questions: If Kamerlingh Onnes had not discovered superconductivity in mercury, could we predict it today? Even more importantly, can state-of-the-art theoretical and computational approaches completely describe superconductivity in mercury? We will show that the answers are not straightforward, since, in mercury, all physical properties relevant for conventional superconductivity, i.e., the electronic structure, phonon dispersion, electron-phonon coupling, and Coulomb matrix elements, are anomalous in some respect.

In the following, we will discuss each of these aspects separately and show how they concur to determine a consistent picture of superconductivity in this fascinating element.

Crystal structure. At ambient conditions, mercury is liquid, but below 235 K it crystallizes in a monatomic rhombohedral lattice, the so-called α phase [26–28], which is commonly accepted as the actual superconducting phase of mercury [9,26–35]. As is known, in mercury even minor structural differences cause dramatic effects on the electronic
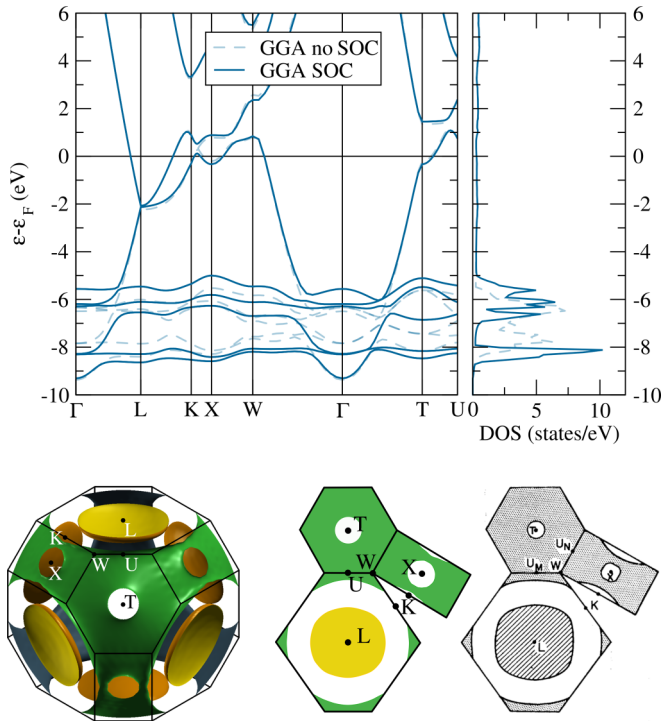
FIG. 1. Top: Electronic band structure and density of states (DOS) of α-Hg, with (solid curve) and without (dashed curve) spin-orbit coupling. Bottom: From left to right, 3D plot of the Fermi surface from fully relativistic calculations; 2D cuts along the BZ boundary are compared with the corresponding experimental cuts from Ref. [32].

and dynamical properties, which are instead perfectly reproduced assuming the experimental lattice structure. See also the Supplemental Material (SM), Secs. I and II [36], for more details on the structural and electronic properties with semilocal functionals [26–28,37,38]. In all calculations of the electronic, dynamical, and superconducting properties, we thus will employ the experimental lattice crystal structure and the generalized gradient approximation (GGA) functional. See SM, Sec. I [36], for more computational details about the software [39–43] and methods used for the calculations [17,44–56].

Electronic structure. We start the discussion from the electronic band structure, shown in Fig. 1 (see also SM, Sec. II [36], for a comparison between local density approximation (LDA) and GGA results). In agreement with previous literature [32,57,58], we find a well-dispersed parabolic band, derived from *s* states, partially hybridized with unoccupied *p* states. In the region between 5.5 and 9 eV below the Fermi level (ε_F), the *s* parabola is tangled with the *d* states. Including relativistic spin-orbit coupling (SOC) causes sizable effects in the *d*-band region and, to a lesser extent, in the vicinity of ε_F. In particular, SOC removes several band degeneracies, for example, around the *L* point and along the $K \rightarrow X$ path; compare the solid and dashed curves in Fig. 1. The resulting density of states (DOS) has a rather interesting shape: A broad feature, corresponding to *s* states, extends from approximately equal to -10 eV to ε_F, and two high, narrow peaks, due to the two groups of spin-orbit split *d* bands, are centered around 6 and 9 eV below ε_F.

To the best of our knowledge, the band structure of mercury has never been measured by angle-resolved photoemission spectroscopy, but indirect evidence of the Fermi surface shape can be inferred from de Haas–van Alphen, magnetoresistance, and cyclotron-resonance measurements [31,32,58]. In the bottom left panel of Fig. 1, we show a three-dimensional (3D) view of the calculated Fermi surface, which comprises two disconnected parts: a tubular network extending throughout the Brillouin zone (BZ) and a disk enclosing the *L* point. Our calculations reproduce the experimental measurements with striking accuracy: Not only the main features, but also finer details, such as the small circular hole pockets around the *X* and *T* points and an elongated hole pocket around the *K* point, are perfectly reproduced.

Vibrational properties. Besides the low-energy electronic structure, DFT-GGA calculations also reproduce with excellent accuracy the phonon dispersions, provided that SOC is included and calculations are performed in the experimental structure. See SM, Sec. III [36], for a comparison between the phonon dispersions obtained with different functionals, with and without SOC.

In the five leftmost panels of Fig. 2, calculated phonon dispersions are compared with the neutron scattering data from Ref. [9]. The phonon spectrum extends up to $\sim$120 cm^{-1} with a pseudogap around 75 cm^{-1} separating transverse and longitudinal modes. The lower transverse branch is very soft and almost flat throughout the whole BZ. Around the *L* point, a further softening occurs: Here, ω_L is only 6.5 cm^{-1}. We find that including relativistic (SOC) effects is crucial for correctly capturing the experimental dispersion in the low-frequency region and obtaining a dynamically stable structure. In fact, without SOC the frequencies of the transverse branch around the *L* point are imaginary; see dashed curves in Fig. 2. This result is consistent with the recent report that relativistic effects are required to explain also the low melting temperature of mercury [59].

Electron-phonon coupling. In the rightmost panel of Fig. 2 we report the phonon DOS and the Éliashberg electron-phonon coupling spectral function. The electron-phonon coupling is almost constant for all phonon modes (see SM, Secs. I and III [36], for the electron-phonon linewidth [60] distribution over the phonon dispersions), but the presence of a soft and weakly dispersive phonon branch causes a pronounced peak at about 15 cm^{-1} in the phonon DOS and in the Éliashberg function. The shape of the $\alpha^2 F(\omega)$ results in a large electron-phonon coupling parameter $\lambda = 1.57$ and a rather small logarithmic-averaged phonon frequency: $\omega_{\log} = 27.3$ K (see also SM, Sec. I [36], for more details).

The agreement of the calculated $\alpha^2 F(\omega)$ with tunneling measurements [9] is excellent: Both the soft-phonon peak at low frequencies (below 25 cm^{-1}) and the reduced coupling of the longitudinal mode at higher frequencies are well reproduced by our calculations. The calculated $\omega_{\log}$ and λ are also in agreement with the corresponding experimental values extracted from tunneling ($\omega_{\log} = 29$ K and $\lambda = 1.6$ [11,13]) and with the specific-heat renormalization data for λ ($\lambda^{sh} \sim 1.56$ [61], 1.66 [62], 1.58 [63], and $\sim$2.0 [64]).

Superconducting properties. Superconducting density functional theory (SCDFT) [65] is an extension of DFT to the SC phase, which was developed with the explicit
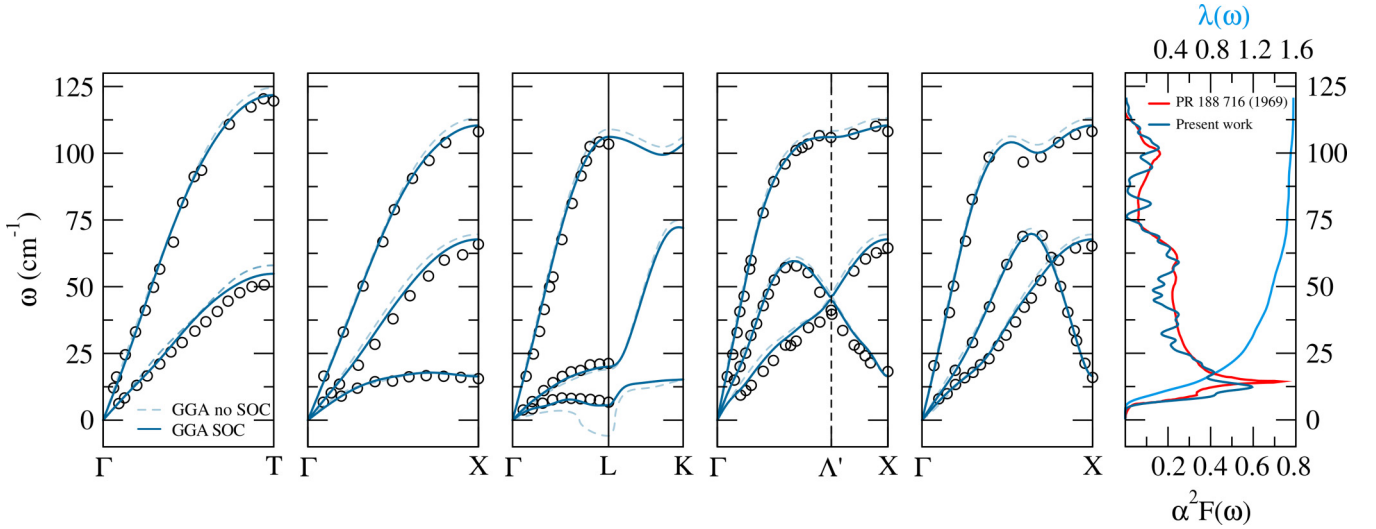
FIG. 2. Left panels: Phonon dispersions of α-Hg along selected high-symmetry lines; solid and dashed curves indicate DFT-GGA calculations with and without SOC. For comparison the experimental measurements from Ref. [9] are reported as open black circles. Rightmost panel: Calculated Éliashberg function $\alpha^2 F(\omega)$ (dark blue; scale at bottom) and frequency-dependent electron-phonon coupling function $\lambda(\omega)$ (light blue; scale at top); experimental tunneling spectra from Ref. [11] are shown in red. PR, *Physical Review*.

purpose [51–54] of treating both the electron-phonon interaction and the Coulomb interaction on an equal footing, eliminating any adjustable parameters, such as the empirical Coulomb pseudopotential μ^*.

The solution of the SCDFT gap equation [17,22] for α-Hg in the static and isotropic approximation, including both electron-phonon and electron-electron interactions, reproduces experimental data with remarkable accuracy, as shown in Fig. 3, where the temperature dependence of the SC gap (at ε_F) obtained in SCDFT (light blue open circles) is compared with tunneling data from Ref. [10] (red squares).

The two curves follow each other rather closely. The critical temperature obtained extrapolating the calculated low-T data is $T_c^{\text{SCDFT}} = 3.84$ K, to be compared with the experimental value $T_c^{\text{expt}} = 4.15$ K (see also SM, Sec. V [36], for more details about the estimation of T_c using semiempirical
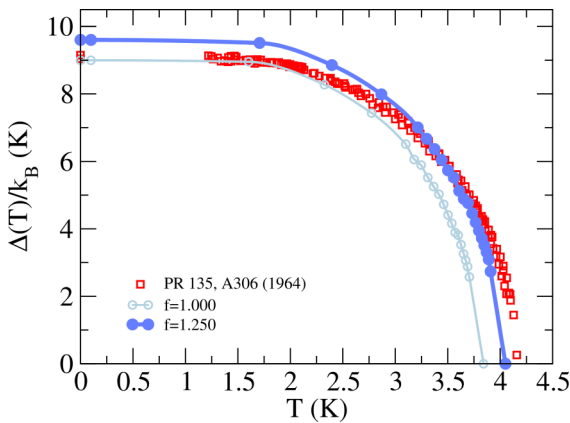

FIG. 3. Comparison between theoretical (light blue circles) and experimental gap [10] (red squares) plotted as a function of temperature. The blue solid circles are obtained with a 1.25 linear scaling of the electronic spectrum, as described in the text.

formulas [5,13,66]). For the BCS ratio $2\Delta(0)/k_B T_c$, SCDFT predicts a value of 4.70, to be compared with experimental values of 4.6 ± 0.2 [67] and 4.60 ± 0.11 [10]. This value places Hg in the strong-coupling regime; its low T_c is due essentially to extremely low phonon frequencies.

Coulomb interaction. In addition to the electron-phonon interaction, SCDFT gives a microscopic insight into the role of the residual Coulomb scattering, an aspect disregarded in most studies of SC, which employ the popular Morel-Anderson approximation. Also, this aspect is strongly anomalous in mercury, as we will show in the following.

In SCDFT, the Coulomb interaction between electrons is described by the isoenergy surface average $V(\varepsilon, \varepsilon')$ of the screened Coulomb matrix elements $V_{i\mathbf{k}, j\mathbf{k}'}$ [55,68]. The SM, Secs. II and IV [36], contains relevant formulas for the electron-phonon and Coulomb interaction and in-depth discussion of the effect of high-energy states on the Coulomb interaction. The effect of $V(\varepsilon, \varepsilon')$ on T_c depends crucially on the energies $\varepsilon, \varepsilon'$ of the two electrons involved in the SC pairing: Coulomb interaction will in fact *suppress* superconductivity if both states lie in energy regions where the SC gap is positive [5,66], i.e., close to ε_F, but can also *favor* it, if one of the two electrons occupies a state at high energies, where the SC gap is negative. In this case, high-energy states will cause a net renormalization (reduction) of the effective Coulomb interaction [22]. A two-dimensional plot of the calculated $V(\varepsilon, \varepsilon')$ function for mercury is shown in Fig. 4; here and in the following, energies are measured with respect to ε_F. Due to the different nature and dispersion of the s and d bands, the diagonal elements of $V(\varepsilon, \varepsilon')$ show a hot spot (blue in top panel of Fig. 4) around -10 eV, corresponding to the bottom of the s parabola in Fig. 1, a squarelike feature, with moderate coupling (green) from -8 to -5 eV, related to d states, and an extended region from zero to high energies (green), related to s and p states. The off-diagonal $\varepsilon = 0$ row, $V(0, \varepsilon')$, which accounts for interband contributions involving the s states at ε_F and all the other states, is nonzero in the low-energy s
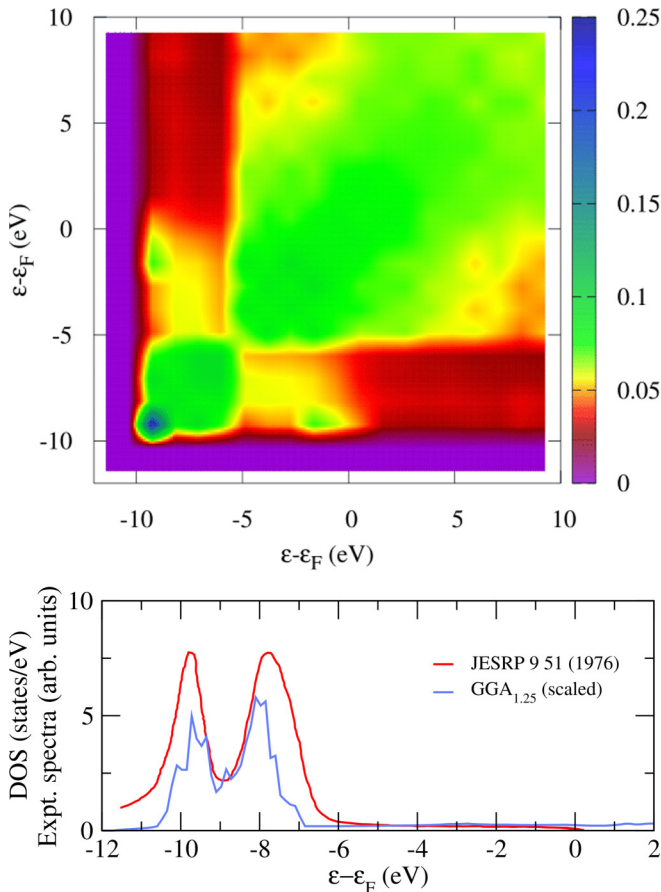
FIG. 4. Top: Two-dimensional plot of the Coulomb potential as a function of the energy with respect to the Fermi level. The color scale expresses the intensity of $V(\varepsilon, \varepsilon')$ in rydbergs. Bottom: Linearly scaled GGA DOS with $f = 1.25$ (see text) compared with the x-ray experiments from Ref. [69]. JESRP, *Journal of Electron Spectroscopy and Related Phenomena*.

region, is very low (nearly zero) for d states ($\varepsilon' < -5$ eV), and is different from zero again only for $\varepsilon' \sim -10$ eV, i.e., near the bottom of the s parabola in Fig. 1.

Based on this energy structure, we expect that the net effect of Coulomb interactions on T_c will be rather weak, due both to low diagonal matrix elements in the low-energy (repulsive) region and to large inter- and intraband contributions in the high-energy (attractive) regions.

The *diagonal* part of the $V(\varepsilon, \varepsilon')$ kernel, evaluated at the Fermi energy ($\varepsilon = 0$), yields the so-called μ parameter. For mercury we obtain $\mu = 0.159$, in line with its neighbors in the periodic table, such as Au and Cd ($\mu = 0.136$ and 0.142, respectively [25]), but much smaller than the average value $\mu = 0.25$ found in most other elemental superconductors such as Pb or Al [25]. Together with the large bandwidth of the s band and the extremely small characteristic phonon frequencies, this translates into a Morel-Anderson pseudopotential $\mu^* = 0.07$, significantly smaller than the standard value $\mu^* = 0.10$ (for more details, see SM, Sec. IV [36]). However, the most interesting anomaly in the Coulomb screening, which cannot be captured by the standard Morel-Anderson approach, is connected to the *off-diagonal* part of the $V(\varepsilon, \varepsilon')$ kernel.

Influence of d states on T_c. Due to the presence of non-negligible off-diagonal s-d Coulomb matrix elements, the calculated T_c in mercury turns out to depend in a critical way on the position of the high-energy d states. This was verified through a simple *gedanken experiment*, in which we solved again the SCDFT equations, leaving all terms unchanged, apart from a scaling of the electronic spectrum, necessary to bring the energy position of the calculated DFT-GGA-SOC d bands in line with experimental x-ray photoemission data [69]. The physical origin of the energy shift between DFT-GGA calculations and experiments is the lack of nonlocal exchange and correlation effects [70–72]; in fact, the shift can be easily removed employing nonlocal functionals, such as the Heyd-Scuseria-Ernzerhof (HSE06) functional [73,74] (see SM, Sec. IV [36], for more details). The main effect can be mimicked by a simple linear scaling of the whole DFT-GGA-SOC spectrum by a constant factor $f = 1.25$, sufficient to bring the calculated spectrum in agreement with the experiment at all energies, as shown in Fig. 4.

Solving the SCDFT equations as a function of temperature with the rescaled spectrum, we obtain the data shown as blue solid circles in Fig. 3: The T_c, obtained from extrapolation of the low-T data, is 4.05 K, with a clear improvement with respect to our previous GGA-SOC result (see SM, Sec. V [36], for a comparison). Although the almost perfect agreement with experiment may be fortuitous, this numerical experiment demonstrates that shifting the position of apparently inert high-energy states can lead to a 10% effect on T_c.

Conclusions. In this Research Letter we carried out a critical study of the superconducting properties of α-mercury, aimed at understanding whether this material, which has played an essential role in superconductivity history, can be described by state-of-the-art computational methods. Our first-principles calculations, validated with an extensive comparison with available experimental literature, demonstrate that state-of-the-art SCDFT can describe the superconducting state of Hg, provided that special care is taken to handle several anomalous electronic and lattice properties. In particular, (i) due to strong nonlocal exchange and correlation effects, structural properties are so poorly described by the standard density functional that in order to obtain meaningful electronic and phonon spectra, all calculations have to be performed in the experimental crystal structure; (ii) SOC effects are extremely strong and crucially affect dynamical stability; and (iii) due to anomalously large off-diagonal s-d matrix elements, the effective Coulomb potential is strongly affected by the energy position of the low-energy d states.

Taken as a whole, our results demonstrate that, even for an apparently simple compound such as mercury, common approximations cannot be applied blindly, as this may cause severe qualitative and quantitative errors. This is a crucial caveat to keep in mind for future high-throughput calculations. We would also like to stress that some of the effects discussed here may appear spectacularly enhanced in high-T_c conventional superconductors, such as the recently discovered superhydrides, where renormalization of the Coulomb interaction has been invoked to justify differences as large as 100 K in the calculated T_c's [75].

[1] H. Kamerlingh Onnes, Commun. Phys. Lab. Univ. Leiden **12**, 120 (1911).

[2] J. Bardeen, L. N. Cooper, and J. R. Schrieffer, Phys. Rev. **108**, 1175 (1957).

[3] A. B. Migdal, Sov. Phys. JETP **7**, 996 (1958).

[4] G. M. Éliashberg, Sov. Phys. JETP **11**, 696 (1960).

[5] P. Morel and P. W. Anderson, Phys. Rev. **125**, 1263 (1962).

[6] G. B. Brandt and J. A. Rayne, Phys. Rev. **148**, 644 (1966).

[7] J. M. Dishman and J. A. Rayne, Phys. Rev. **166**, 728 (1968).

[8] A. E. Dixon and W. R. Datars, Phys. Rev. **175**, 928 (1968).

[9] W. A. Kamitakahara, H. G. Smith, and N. Wakabayashi, Ferroelectrics **16**, 111 (1977).

[10] S. Bermon and D. M. Ginsberg, Phys. Rev. **135**, A306 (1964).

[11] W. N. Hubin and D. M. Ginsberg, Phys. Rev. **188**, 716 (1969).

[12] W. L. McMillan, Phys. Rev. **167**, 331 (1968).

[13] P. B. Allen and R. C. Dynes, Phys. Rev. B **12**, 905 (1975).

[14] S. Baroni, S. de Gironcoli, A. Dal Corso, and P. Giannozzi, Rev. Mod. Phys. **73**, 515 (2001).

[15] S. Y. Savrasov and D. Y. Savrasov, Phys. Rev. B **54**, 16487 (1996).

[16] F. Giustino, Rev. Mod. Phys. **89**, 015003 (2017).

[17] A. Sanna, C. Pellegrini, and E. K. U. Gross, Phys. Rev. Lett. **125**, 057001 (2020).

[18] C. J. Pickard and R. J. Needs, J. Phys.: Condens. Matter **23**, 053201 (2011).

[19] S. Curtarolo, G. L. W. Hart, M. B. Nardelli, N. Mingo, S. Sanvito, and O. Levy, Nat. Mater. **12**, 191 (2013).

[20] C. J. Pickard, Phys. Rev. B **99**, 054102 (2019).

[21] A. R. Oganov, C. J. Pickard, Q. Zhu, and R. J. Needs, Nat. Rev. Mater. **4**, 331 (2019).

[22] J. A. Flores-Livas, L. Boeri, A. Sanna, G. Profeta, R. Arita, and M. Eremets, Phys. Rep. **856**, 1 (2020).

[23] N. W. Ashcroft, Phys. Rev. Lett. **92**, 187002 (2004).

[24] L. Boeri, R. G. Hennig, P. J. Hirschfeld, G. Profeta, A. Sanna, E. Zurek, W. E. Pickett, M. Amsler, R. Dias, M. Eremets, C. Heil, R. Hemley, H. Liu, Y. Ma, C. Pierleoni, A. Kolmogorov, N. Rybin, D. Novoselov, V. I. Anisimov, A. R. Oganov *et al.*, J. Phys.: Condens. Matter **34**, 183002 (2022).

[25] M. Kawamura, Y. Hizume, and T. Ozaki, Phys. Rev. B **101**, 134511 (2020).

[26] L. Pauling, J. Am. Chem. Soc. **69**, 542 (1947).

[27] C. S. Barrett, Acta Crystallogr. **10**, 58 (1957).

[28] *CRC Handbook of Chemistry and Physics* 78th ed., edited by D. R. Lide (CRC, New York, 1997).

[29] O. Schulte and W. B. Holzapfel, Phys. Rev. B **48**, 14009 (1993).

[30] C. A. Swenson, Phys. Rev. **111**, 82 (1958).

[31] G. Brandt and J. Rayne, Phys. Lett. **15**, 18 (1965).

[32] S. C. Keeton and T. L. Loucks, Phys. Rev. **152**, 548 (1966).

[33] O. Schulte and W. B. Holzapfel, Phys. Rev. B **53**, 569 (1996).

[34] J. A. Moriarty, Phys. Lett. A **131**, 41 (1988).

[35] S. Biering and P. Schwerdtfeger, Theor. Chem. Acc. **130**, 455 (2011).

[36] See Supplemental Material at http://link.aps.org/supplemental/10.1103/PhysRevB.106.L180501 for computational details, details of the crystal structure, calculations of electronic and dynamical properties in both LDA and GGA approximations, an estimation of the superconducting critical temperature with semiempirical formulas, the effect of the screened Coulomb interaction on the band structure, and the estimation of the superconducting critical temperature.

[37] N. Gaston, B. Paulus, K. Rosciszewski, P. Schwerdtfeger, and H. Stoll, Phys. Rev. B **74**, 094102 (2006).

[38] J. P. Perdew, K. Burke, and M. Ernzerhof, Phys. Rev. Lett. **77**, 3865 (1996).

[39] P. Giannozzi, S. Baroni, N. Bonini, M. Calandra, R. Car, C. Cavazzoni, D. Ceresoli, G. L. Chiarotti, M. Cococcioni, I. Dabo, A. D. Corso, S. de Gironcoli, S. Fabris, G. Fratesi, R. Gebauer, U. Gerstmann, C. Gougoussis, A. Kokalj, M. Lazzeri, L. Martin-Samos *et al.*, J. Phys.: Condens. Matter **21**, 395502 (2009).

[40] P. Giannozzi Jr, O. Andreussi, T. Brumme, O. Bunau, M. B. Nardelli, M. Calandra, R. Car, C. Cavazzoni, D. Ceresoli, M. Cococcioni, N. Colonna, I. Carnimeo, A. D. Corso, S. de Gironcoli, P. Delugas, R. A. DiStasio Jr, A. Ferretti, A. Floris, G. Fratesi, G. Fugallo *et al.*, J. Phys.: Condens. Matter **29**, 465901 (2017).

[41] G. Kresse and J. Furthmüller, Comput. Mater. Sci. **6**, 15 (1996).

[42] G. Kresse and J. Furthmüller, Phys. Rev. B **54**, 11169 (1996).

[43] G. Kresse and D. Joubert, Phys. Rev. B **59**, 1758 (1999).

[44] H. J. Monkhorst and J. D. Pack, Phys. Rev. B **13**, 5188 (1976).

[45] D. R. Hamann, Phys. Rev. B **88**, 085117 (2013).

[46] D. R. Hamann, Phys. Rev. B **95**, 239906(E) (2017).

[47] M. van Setten, M. Giantomassi, E. Bousquet, M. Verstraete, D. Hamann, X. Gonze, and G.-M. Rignanese, Comput. Phys. Commun. **226**, 39 (2018).

[48] N. Marzari and D. Vanderbilt, Phys. Rev. B **56**, 12847 (1997).

[49] I. Souza, N. Marzari, and D. Vanderbilt, Phys. Rev. B **65**, 035109 (2001).

[50] M. Calandra, G. Profeta, and F. Mauri, Phys. Rev. B **82**, 165111 (2010).

[51] L. N. Oliveira, E. K. U. Gross, and W. Kohn, Phys. Rev. Lett. **60**, 2430 (1988).

[52] M. Lüders, M. A. L. Marques, N. N. Lathiotakis, A. Floris, G. Profeta, L. Fast, A. Continenza, S. Massidda, and E. K. U. Gross, Phys. Rev. B **72**, 024545 (2005).

[53] M. A. L. Marques, M. Lüders, N. N. Lathiotakis, G. Profeta, A. Floris, L. Fast, A. Continenza, E. K. U. Gross, and S. Massidda, Phys. Rev. B **72**, 024546 (2005).

[54] A. Floris, G. Profeta, N. N. Lathiotakis, M. Lüders, M. A. L. Marques, C. Franchini, E. K. U. Gross, A. Continenza, and S. Massidda, Phys. Rev. Lett. **94**, 037004 (2005).

[55] A. Sanna, J. A. Flores-Livas, A. Davydov, G. Profeta, K. Dewhurst, S. Sharma, and E. K. U. Gross, J. Phys. Soc. Jpn. **87**, 041012 (2018).

[56] G. Marini, P. Barone, A. Sanna, C. Tresca, L. Benfatto, and G. Profeta, Phys. Rev. Mater. **3**, 114803 (2019).

[57] H. Jansen, A. Freeman, M. Weinert, and E. Wimmer, Phys. Rev. B **28**, 593 (1983).

[58] S. Deng, A. Simon, and J. Köhler, Angew. Chem., Int. Ed. **37**, 640 (1998).

[59] F. Calvo, E. Pahl, M. Wormit, and P. Schwerdtfeger, Angew. Chem., Int. Ed. **52**, 7583 (2013).

[60] M. Calandra and F. Mauri, Phys. Rev. Lett. **101**, 016401 (2008).

[61] B. J. C. van der Hoeven and P. H. Keesom, Phys. Rev. **135**, A631 (1964).

[62] N. E. Phillips, M. H. Lambert, and W. R. Gardner, Rev. Mod. Phys. **36**, 131 (1964).

[63] D. K. Finnemore and D. E. Mapother, Phys. Rev. **140**, A507 (1965).

[64] D. K. Finnemore, D. E. Mapother, and R. W. Shaw, Phys. Rev. **118**, 127 (1960).

[65] A. Davydov, A. Sanna, C. Pellegrini, J. K. Dewhurst, S. Sharma, and E. K. U. Gross, Phys. Rev. B **102**, 214508 (2020).

[66] D. J. Scalapino, J. R. Schrieffer, and J. W. Wilkins, Phys. Rev. **148**, 263 (1966).

[67] P. L. Richards and M. Tinkham, Phys. Rev. **119**, 575 (1960).

[68] S. Massidda, F. Bernardini, C. Bersier, A. Continenza, P. Cudazzo, A. Floris, H. Glawe, M. Monni, S. Pittalis, G. Profeta, A. Sanna, S. Sharma, and E. K. U. Gross, Supercond. Sci. Technol. **22**, 034006 (2009).

[69] S. Svensson, N. Martensson, E. Basilier, P. Malmqvist, U. Gelius, and K. Siegbahn, J. Electron Spectrosc. Relat. Phenom. **9**, 51 (1976).

[70] T. Rangel, D. Kecik, P. E. Trevisanutto, G.-M. Rignanese, H. Van Swygenhoven, and V. Olevano, Phys. Rev. B **86**, 125125 (2012).

[71] A. Marini, R. Del Sole, and G. Onida, Phys. Rev. B **66**, 115101 (2002).

[72] A. Svane, N. E. Christensen, M. Cardona, A. N. Chantis, M. van Schilfgaarde, and T. Kotani, Phys. Rev. B **84**, 205205 (2011).

[73] J. Heyd, G. E. Scuseria, and M. Ernzerhof, J. Chem. Phys. **118**, 8207 (2003).

[74] J. Heyd, G. E. Scuseria, and M. Ernzerhof, J. Chem. Phys. **124**, 219906 (2006).

[75] I. A. Troyan, D. V. Semenok, A. G. Kvashnin, A. V. Sadakov, O. A. Sobolevskiy, V. M. Pudalov, A. G. Ivanova, V. B. Prakapenka, E. Greenberg, A. G. Gavriliuk, I. S. Lyubutin, V. V. Struzhkin, A. Bergara, I. Errea, R. Bianco, M. Calandra, F. Mauri, L. Monacelli, R. Akashi, and A. R. Oganov, Adv. Mater. **33**, 2006832 (2021).